2023

Conformal Electrodeposition of Antimicrobial Hydrogels Formed by Self-Assembled Peptide Amphiphiles

Gervasio Zaldivar

Jiachen Feng

Leonardo Lizarraga

Yafan Yu

Luana de Campos

See next page for additional authors

Authors

Gervasio Zaldivar, Jiachen Feng, Leonardo Lizarraga, Yafan Yu, Luana de Campos, Kelly Mari Pires de Oliveira, Kurt Piepenbrink, Martin Conda-Sheridan, and Mario Tagliazucchi

ADVANCED MATERIALS INTERFACES
Open Access
www.advmatinterfaces.de

Conformal Electrodeposition of Antimicrobial Hydrogels Formed by Self-Assembled Peptide Amphiphiles

Gervasio Zaldivar, Jiachen Feng, Leonardo Lizarraga, Yafan Yu, Luana de Campos, Kelly Mari Pires de Oliveira, Kurt H. Piepenbrink, Martin Conda-Sheridan, and Mario Tagliazucchi**

The colonization of biomedical surfaces by bacterial biofilms is concerning because these microorganisms display higher antimicrobial resistance in biofilms than in liquid cultures. Developing antimicrobial coatings that can be easily applied to medically-relevant complex-shaped objects, such as implants and surgical instruments, is an important and challenging research direction. This work reports the preparation of antibacterial surfaces via the electrodeposition of a conformal hydrogel of self-assembling cationic peptide-amphiphiles (PAs). Hydrogels of three PAs are electrodeposited: $C_{16}K_2$, $C_{16}K_3$, and $C_{18}K_2$, where C_n is an alkyl chain of *n* methylene groups and K_m is an oligopeptide of *m* lysines. The processing variables (electrodeposition time, potential, pH, salt concentration, agitation) enable fine control of film thickness, demonstrating the flexibility of the method and allowing to unravel the mechanisms underlying electrodeposition. The electrochemically prepared hydrogels inhibit the growth of *Staphylococcus aureus*, *Escherichia coli*, and *Pseudomonas aeruginosa* in agar plates, and prevent the formation of biofilms of *Acinetobacter baumannii* and *P. aeruginosa* and the formation of *A. baumannii* colonies in solid media. $C_{16}K_2$ and $C_{16}K_3$ hydrogels outperform the antimicrobial activity of those of $C_{18}K_2$ while maintaining good compatibility with human cells.

1. Introduction

Bacterial infections are a global challenge because of the emergence of strains resistant to common antibiotics.[1] In the 2019 World Health Organization (WHO) report,[1] bacterial pathogens resistant to first-line antimicrobials that are commonly found in healthcare facilities were considered a top priority. Some of these troublesome microorganisms have been named the ESKAPE pathogens (*Enterococcus faecium, Staphylococcus aureus, Klebsiella pneumoniae, Acinetobacter baumannii, Pseudomonas aeruginosa,* and *Enterobacter spp*). Moreover, resistance to antibiotics can be especially worrisome in hospital-acquired infections.[2,3] According to the WHO, one effective way to fight these infections is controlling the cleanness of the medical material and work environment.[4] Furthermore, surgical implants (made of titanium or surgical steel) are

G. Zaldivar, M. Tagliazucchi
Universidad de Buenos Aires
Facultad de Ciencias Exactas y Naturales
Departamento de Química Inorgánica Analítica y Química Física
CONICET-Universidad de Buenos Aires
Facultad de Ciencias Exactas y Naturales
Instituto de Química de los Materiales
Ambiente y Energía (INQUIMAE)
Buenos Aires C1428EGA, Argentina
E-mail: mario@qi.fcen.uba.ar

J. Feng, L. de Campos, M. Conda-Sheridan
Department of Pharmaceutical Sciences
College of Pharmacy
University of Nebraska Medical Center
Omaha, NE 68198-6125, USA
E-mail: martin.condasheridan@unmc.edu

The ORCID identification number(s) for the author(s) of this article can be found under https://doi.org/10.1002/admi.202300046.

DOI: 10.1002/admi.202300046

L. Lizarraga
Biopolymers Group
Centro de Investigaciones en Bionanociencias (CIBION-CONICET)
Buenos Aires C1425FQD, Argentina

Y. Yu
Department of Biochemistry and Department of Food Science and Technology
University of Nebraska-Lincoln
Lincoln, NE 68588, USA

K. M. P. de Oliveira
Faculty of Biological and Environmental Science
Federal University of Grande Dourados
Dourados, MS 79804–970, Brazil

K. H. Piepenbrink
Department of Biochemistry
Department of Food Science and Technology
Department of Chemistry
Nebraska Food for Health Center
Center for Integrated Biomolecular Communication
University of Nebraska-Lincoln
Lincoln, NE 68588, USA

often colonized by bacteria after their insertion[5] leading to delays in patient recovery[6] or even their removal and replacement.[7] Avoiding bacterial biofilms on these surfaces is of paramount importance, since biofilms enhance the resistance of bacteria against the natural defenses of the organism and common antibiotics,[8] often leading to persistent infections.[9] The use of antimicrobial hydrogel coatings is an interesting strategy to prevent the colonization of medical material.[10–12] For example, the manual application (i.e., using a brush) of an antimicrobial polymer-based hydrogel containing gentamycin and vancomycin reduced by 86% the bacterial colonization of titanium substrates.[12] However, manual application onto complex-shaped devices, such as screws or stents, can be difficult and ineffective. In this context, it is necessary to develop technologies to produce conformal antimicrobial coatings on complex-shaped surfaces.

Many biomedical-relevant substrates are metallic, and, therefore, electrodeposition can be used to prepare conformal coatings, that is, coatings that adapt to the shape of the surface. The electrodeposition of hydrogels involves applying an electrochemical potential to the targeted substrate. The applied potential changes the solution conditions near the substrate and locally triggers gelation.[13,14] The electrodeposition of bioinactive polymeric gels embedded with small antimicrobial molecules has been explored in the past.[15–20] In this work, we report the electrodeposition of low-molecular-weight gelators, that is, peptide-amphiphiles (PAs). Even though the electrodeposition of low molecular weight gelators has been reported,[21–23] this is the first time this approach is used to develop antimicrobial coatings and that such technique is applied to PAs.

PAs are molecules formed by a hydrophobic moiety (usually a single alkyl chain) linked to a hydrophilic peptide region that is generally charged.[24–27] Due to their amphiphilic nature, PAs self-assemble into a broad variety of nanostructures in water solution, including spherical micelles,[28–31] cylindrical fibers of different lengths,[27,30–32] and long, planar nanoribbons.[29–32] In addition to this morphological richness, PAs show highly adaptable functionality because the peptide moiety can be easily tailored to be bioactive. These remarkable characteristics have triggered great interest in the applications of PAs in regenerative medicine,[33–35] drug and protein delivery with specific cell targeting,[36–39] and treatments against cancer[40,41] and bacterial infections.[42–44] Furthermore, PAs are used in the cosmetic industry as skin regenerators[45] and antimicrobial agents[46] under different names, such as palmitoyl oligopeptides.

Antimicrobial PAs are a type of antimicrobial peptide (AMPs) characterized by the presence of cationic amino acids (e.g., lysine and arginine) in their peptide region. The antibacterial activity of cationic PAs involves the interaction between the positive groups in the peptide region and the negatively charged bacterial membrane, which disrupts the membrane and leads to cell death.[42,43,47,48] This mechanism is expected to reduce the development of bacterial resistance due to the great metabolic cost required to repair the membrane's molecular elements and the evolutionary barrier to drastically change the bacterial membrane composition. While this antimicrobial mechanism is common to most AMPs, PAs have some key advantages over regular peptides. Firstly, PA aggregates are expected to be more resistant to proteolytic hydrolysis than isolated peptides. Metabolic degradation usually leads to limited bioavailability and a short half-life.[49] Secondly, the morphology and bioactivity of PA aggregates can be straightforwardly tuned by changing their chemical structure (length of the alkyl tail and sequence of amino acids) or chemical environment.[31,42] For example, the morphology of the aggregates of lysine-based PAs changes from spherical micelles to elongated objects (fibers or nanoribbons) with increasing pH.[31,32] The morphology of these aggregates can also be controlled by the length of the alkyl tail or the number of lysines forming the peptide region.

In this work, we electrodeposited antimicrobial hydrogels made of self-assembled cationic PA nanofibers of formula C_nK_m. Some compounds of this family are known to be antimicrobial[42,43,49] and their mechanism of action, cytotoxicity, and biocompatibility have been already comprehensively investigated.[42,43,47,50,51] In a previous study,[42] we used scanning electron microscopy (SEM), confocal microscopy, and flow cytometry to characterize the antimicrobial mechanisms of methicillin-resistant staphylococcus aureus (MRSA) and *Escherichia coli* K12 strains. It was shown that PAs of the family C_nK_m increased the permeability and ultimately disrupted bacterial membranes, leading to lysis and death, in agreement with findings from other groups.[43,47] The most potent antimicrobials in the family C_nK_m are also the most cytotoxic ones,[42,50,51] but we have shown that some compounds of this family exhibit good therapeutic indexes ($LD_{50}/MIC > 10$) for *E. coli* and *S. aureus*.[42]

Interestingly, some members of the C_nK_m family form hydrogels due to a pH-driven transition from spherical micelles (or free PAs in solution) at acidic pHs to elongated objects at basic pHs.[31,32] In this work, we exploited this property to engineer a method to electrodeposit PA hydrogels. The electro-reduction of water by an electrode immersed in a PA solution increases the pH in the proximity of the electrode surface. This local pH increase drives the PA self-assembly into nanofibers and, ultimately, produces a gel on the surface. We demonstrate that the method allows the conformal deposition of the gels on complex-shaped electrodes. Tuning the applied potential, exposition time, initial pH, and/or salt concentration of the solution provides precise control over the amount of electrodeposited hydrogel. Electrodeposited PA hydrogels effectively inhibit the growth of different bacterial strains in agar plates and, more importantly, they inhibit the growth of bacterial biofilms on coated surfaces. Our approach has some crucial advantages over existing antimicrobial coatings based on polymeric gels containing traditional antibiotics, namely: a) our PA hydrogels are intrinsically antimicrobial; thus, they act both as structural building blocks and bioactive compounds. This feature simplifies product formulation and enhances the local concentration of the bioactive material on the surface when compared to previous formulations in which a bio-inactive gel scaffold loads the bioactive compounds.[52,53] b) Bacterial resistance against PAs is expected to be less likely (although possible)[54] than against traditional antibiotics because PAs act by disrupting bacterial membranes.[55,56] c) Unlike some polymeric gels, supramolecular gels dissolve slowly (in the scale of hours or days, as we show below), and PAs are slowly enzymatically degraded, thereby facilitating their removal from the organism.[57,58] d) PA hydrogels are self-repairing,[59] and e) the electrodeposition of PA hydrogels

does not require any chemical modification of the surfaces or polymerization reactions involving potentially toxic chemical reactants. Finally, since PAs are molecules with impressive versatility, the electrodeposition approach reported here could also lead to coatings for applications in fields such as biosensors and regenerative medicine.[37,60,61]

2. Experimental Section

2.1. Synthesis of Peptide Amphiphiles

The synthesis of $C_{18}K_2$, $C_{16}K_2$, and $C_{16}K_3$ was performed using standard Fmoc solid-phase peptide synthesis, following the procedure of previous works.[31] Amino acids and Rink amide resins were supplied by P3Bio and solvents by Fisher. Characterization was performed with MALDI (Figures S1–S3, Supporting Information).

2.2. Atomic Force Microscopy (AFM)

Chemical hydrogels were prepared by adding 1 µL of NaOH 1 M to 5 µL of a 5 wt.% PA solution. Electrogels were directly electrodeposited on AFM steel disks of 10 mm diameter in conditions where the gels have ≈5 wt.% PA concentration. Gels were dried and AFM images were acquired using a Bruker Multimode 8 SPM (Santa Barbara, CA, USA) with a NanoScope V Controller (Santa Barbara, CA, USA). The AFM images were acquired in the intermittent mode using silicon tips doped with antimony, with a spring constant of 42 N m^{-1} and a resonance frequency of 320 kHz. Typically, areas of 2×2 μm^2 were scanned. The image analysis was performed using Gwyddion version 2.46 (Brno, Czech Republic). Average surface roughness was determined from AFM height images.[62]

2.3. Height, Mass, and Water Percentage of the Electrodeposited Gel

To measure the height, the PA gels were electrodeposited on gold disk electrodes (see height definition in Figure 2A), photographed with a magnifying lens and analyzed using ImageJ.[63] To measure the mass, the gels were mechanically detached from the electrode and weighed. The mass of the freshly prepared gel is referred to as the "wet" mass (m_{wg}) and that of the dried gel (lyophilized for at least 6 h) as the dry mass (m_{dg}). The weight percentage of water in the gel was determined as $100\% \times (m_{wg} - m_{dg})/m_{wg}$.

2.4. Electrodeposition

All electrodepositions were performed using a three-electrode setup. A platinum mesh was used as the counter electrode and an Ag/AgCl KCl 3 M electrode as the reference. Electrochemical depositions were carried either with a Teq3 potentiostat (nanoTeq, Argentina) or with an electrochemical analyzer CHI6011B (CH Instruments, USA).

2.5. Rheological Properties

The storage modulus (G'), loss modulus (G''), and complex viscosity (η^*) of the PA hydrogels with a concentration of 2.5 wt.% were measured in the oscillation frequency sweep mode of a DHR-2 rheometer with a 20-mm parallel-plate geometry (TA Instrument, New Castle, DE). The sample was uniformly loaded on the Peltier plate of the rheometer using a syringe. The thickness of the sample was set to 1000 µm, the strain to 1% and the temperature to 25 °C. G', G'', and η^* were measured in the oscillatory frequency range from 0.1 to 100 rad·s^{-1} for the three compounds.

2.6. Determination of the Inhibition Zone (Kirby Bauer Assay)

Zone-of-inhibition assays were performed on agar plates inoculated with *S. aureus* USA 300 JE2, *E. coli* K12, and *P. aeruginosa* ATCC 27853 by adapting previously reported protocols to determine the zone of inhibition of hydrogels.[64,65] 35 µL of 10^9 CFU mL^{-1} bacterial culture prepared in Muller–Hinton broth (MHB) was streaked evenly on each section of a 3-section plate filled with Muller–Hinton agar (MHA). A 5-µL droplet of PA-gel was deposited on each section of the plate previously inoculated with bacteria, and the plates were incubated at 37 °C overnight. The inhibition zones around the hydrogels (zones lacking bacterial growth) were measured by taking photographs and analyzing them with the software ImageJ.[63] PA gels were prepared through two different methods. Electrogels were prepared by electrochemical deposition of the PAs on an electrode by applying a reductive potential (see Section 3.1). Chemical gels were prepared by adding a 1 M NaOH solution to a PA solution in water until gelation. Paper disks embedded with pure water and 1 M NaOH aqueous solution were used as negative controls.

2.7. Inhibition of Biofilm Growth

Hydrogels of $C_{16}K_2$, $C_{18}K_2$, and $C_{16}K_3$ were formed at the bottom of a 96-well microplate by rapid mixing of 2 µL of 1 M NaOH, 6 µL of a 2.5 wt.% PA solution, and 18 µL of distilled H_2O; control wells were inoculated with 30 µL of 1 M NaOH solution at an identical final concentration (67 mM). Gels formed within minutes and were left overnight at 4 °C. The following day, the wells were washed three times with 100 µL of Luria broth without salt. Wells were inoculated with 100 µL of bacterial culture (1:10 from an overnight saturation growth of either *A. baumannii* 17978 or *P. aeruginosa* PAO1), and static biofilms were allowed to grow at 37 °C for 24 h, after which all liquid was removed. Staining biofilms with standard methods to measure the formation of the extracellular matrix was complicated by the hydrophobicity of the hydrogels, which bound crystal violet, Gram's safranin, and Congo red, robustly causing high background rates. To assess biofilm formation, wells were washed three times with PBS and inoculated with 100 µL of fresh growth media. After 18 h at 37 °C, planktonic outgrowth from biofilms was measured by OD_{600} of the supernatant (diluted 1:5 in fresh media), and

A_{490} of the same supernatant after centrifugation to remove bacterial cells.

2.8. β-Lactamase Assay

Given the difficulty to measure the formation of the extracellular matrix using standard dyes, a colorimetric assay using nitrocefin was used to measure the growth of *A. baumannii* biofilms. In this assay, biofilms were grown as described above and incubated with a 20 μM solution of nitrocefin (Thermofisher) in PBS. Nitrocefin was a cephalosporin analog that was yellow when dissolved in an aqueous solution but produces a red fragment when cleaved by β-lactamase enzymes.[66] The β-lactamase activity, as a proxy for bacteria viability, was measured by the increase in the extinction coefficient at 600 nm and the corresponding decrease at 400 nm using a Synergy H1 plate reader (Biotek).

2.9. Solid Media Assay

The ability of hydrogels to inhibit growth in solid media was measured using chromogenic media. Media selective for *A. baumannii* and related species (CHROMagar) was impregnated with PA solutions + 1% in 0.03 M NaOH (a 0.03 M NaOH solution was used as a control) and were allowed to polymerize in a grid pattern. Five microliters of exponential phase *A. baumannii* AB5075 broth culture were then added to each spot on the grid. Colony formation by *A. baumannii* was assessed by the appearance of red colonies on the chromogenic media and measured using mean intensity as determined by ImageJ.[67]

2.10. Cytotoxicity Studies

HEp-2 and HEK 293 cells were used as model cell lines to assess the cytotoxicity of the PA solution and hydrogel. DMEM media (Gibco) with 10% fetal bovine serum, 1% penicillin/streptomycin, and 200 mmol L-glutamine was used to culture HEK-293 cell line; DMEM media (Gibco) with 10% fetal bovine serum, 10 μg mL^{-1} gentamicin was used to culture HEp-2 cell line. Both cells were incubated in a 5% CO_2 humidified environment. The cells were then seeded in 96-well plates at a density of 5000 cells per well and incubated for 24 h. After that, PA solutions were added into cell cultures at a concentration range from 128 to 8 μg ml^{-1} in triplicate. To evaluate the cytotoxicity of chemical hydrogels, they were first prepared by the addition of 1 M NaOH to a 2.5% w/w PA solution until gelation and then introduced into the 96-well plates. After 20 h, the medium was removed and washed with 100 μL of PBS, and 100 μL of new media was added following. Finally, the cell viability was measured using XTT assay according to the manufacturer's protocol (CyQUANT XTT cell viability assay, Invitrogen, ref. X12223). The 450 nm absorbance readings were examined and corrected by a Thermo Fisher Scientific multiscan FC microplate photometer. A control without added PA was used to calculate the percentage of cell viability. A NaOH solution was also tested at the same concentration used in the hydrogel preparation, which showed no cytotoxicity.

3. Results and Discussion

3.1. Electrodeposition of PA Hydrogels

The hydrogel electrodeposition reported in this work is based on the generation of a pH gradient by an electrochemical reaction, see **Figure 1**A. The method consists in applying a reductive potential to an inert electrode immersed in a PA solution at low pH. The reductive potential leads to an increase in the local pH on the surface of the electrode, likely due to the reduction of water.

$$2H_2O(l) + 2e^- \rightarrow 2OH^-(aq) + H_2(g) \quad (1)$$

The reduction of dissolved oxygen and nitrates from the supporting electrolyte[68] can also contribute to the basification process.

In our method, the local pH increase triggers the PA's morphological transition from spheres to cylindrical fibers, as demonstrated by previous TEM,[31] AFM,[31] cryo-TEM,[32] and SAXS[32] studies. This transition drives the formation of the gel. Therefore, to be suitable for electrodeposition, the PA must aggregate into spheres at low pH and undergo a transition to elongated objects (cylindrical fibers and/or planar ribbons) with increasing pH. To achieve this, we considered PAs of the chemical structure C_nK_m, see Figure 1B. The compounds $C_{16}K_3$ and $C_{16}K_2$ have already been shown to exhibit the behavior required for electrodeposition.[31,32] As an example, Figure 1C,D show the morphology diagram for $C_{16}K_3$ calculated using a molecular theory[31] as a function of pH and added salt concentration, and the atomic force microscopy images of a 4 mM solution at pH = 8 and 10 (data reproduced from ref. [31]). In the case of $C_{16}K_2$, the pH-induced sphere-to-fiber transition was also demonstrated by cryo-TEM and SAXS by Gao et al.[32] We also prepared the PA $C_{18}K_2$[69] and demonstrated the pH-induced sphere-to-fiber transition using TEM (Figure S5, Supporting Information). At high enough concentrations, the fibers of these PAs obtained in basic media entangle and form gels. For example, Figure 1E shows pictures of a 2.5 wt.% $C_{16}K_3$ solution at low pH (solution) and high pH (gel). The rheological properties of the gels are reported in Supporting Information, (Figure S4, Supporting Information). In summary, we synthesized and used in this work the PAs $C_{16}K_2$, $C_{16}K_3$, and $C_{18}K_2$,[69] which transition from spheres to elongated objects (fibers and then ribbons) with increasing pH and, thus, are suitable for electrodeposition. Other PAs of the family C_nK_m do not meet the requirements for our method, for example, the compound $C_{16}K$ forms bilayer structures (planar ribbons and nanotubes) at all pH values.[70]

The sphere-to-fiber transition for $C_{16}K_3$, $C_{16}K_2$, and $C_{18}K_2$ occurs at pH ≈ 9, 7.5, and 6, respectively (determined from TEM/cryo-TEM, see refs. [31,32], and Figure S5, Supporting Information, respectively). The minimum concentration of gelation was around 2 wt.% for the three compounds. We successfully prepared electrodeposited gels for these three PAs on electrodes of different shapes and made of different materials, such as stainless steel, aluminum, gold, and indium tin oxide. **Figure 2**A shows a gold disk electrode (diameter = 3 mm, upper panel) and stainless-steel mesh (lower panel) before the

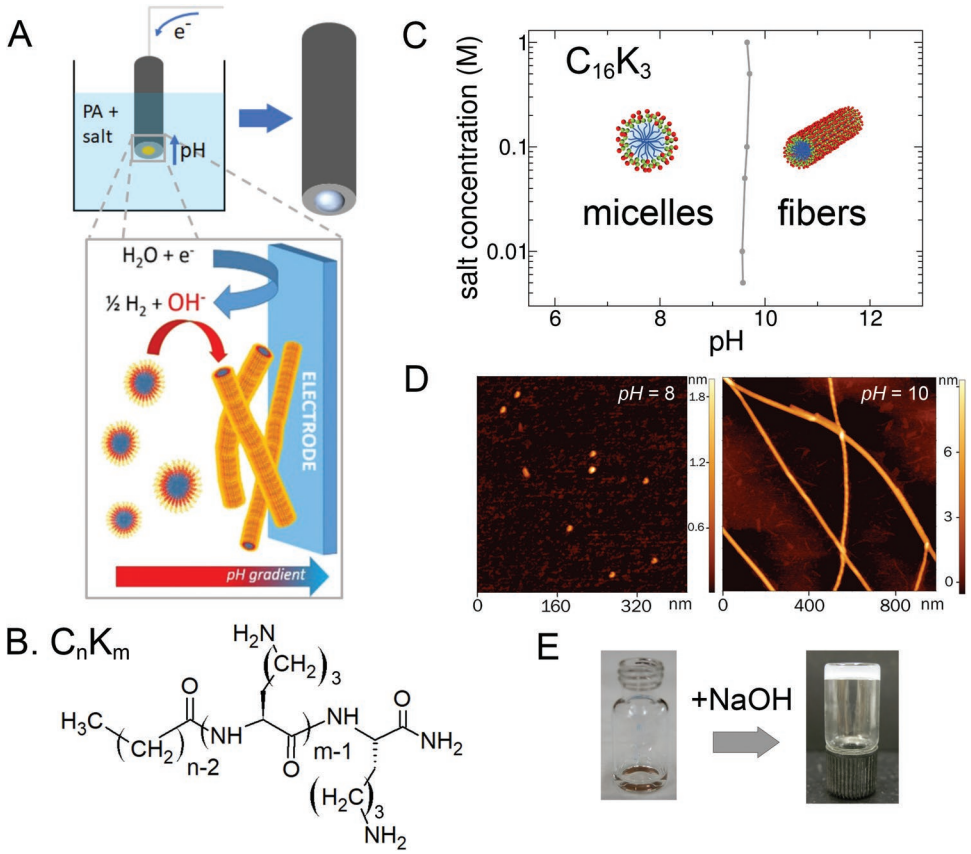

Figure 1. A) Scheme of the electrodeposition method. A reductive potential applied to the electrode produces the electroreduction of water, releasing hydroxyl ions that trigger a sphere-to-fiber transition on the electrode surface. The PA fibers entangle, forming a hydrogel. B) Molecular structures of the family of PAs studied in this work. C) Morphology diagram of $C_{16}K_3$ calculated with a molecular theory in ref. [31] as a function of pH and salt concentration (Reproduced with permission.[31] Copyright 2019, American Chemical Society.). D) AFM images of $C_{16}K_3$ at pH = 8 (spherical micelles) and pH 10 (nanofibers) (Reproduced with permission.[31] Copyright 2019, American Chemical Society.). E) $C_{16}K_3$ solution at pH ≈ 7 (left) and pH > 10 (right) showing the gelation process.

deposition of $C_{16}K_3$. Figure 2B shows the same substrates after the electrodeposition of $C_{16}K_3$. The successful electrodeposition on the stainless-steel mesh demonstrates the capabilities of the technique to produce conformal hydrogel coatings on complex-shaped electrodes.

3.2. Characterization of the Electrodeposited Hydrogels

We studied the nanostructure of the gels using atomic force microscopy (AFM). **Figure 3**A shows an AFM image of a $C_{16}K_3$ gel formed by adding NaOH to a 5 wt.% PA solution (hereafter, we will refer to the gels prepared with this method as "chemical gels"). Figure 3B shows an AFM image of a $C_{16}K_3$ gel directly electrodeposited on a stainless-steel flat surface ("electrogel"). Both images exhibit similar characteristics, that is, there is a network of entangled nanofibers with diameters of ≈10 nm. The root mean square (RMS) roughness was the same for both samples (15 ± 5 nm). We conclude that there are no significant differences between the nanostructure of the chemical gels and the electrogels (note that the concentration of the PA in both gels is expected to be approximately equal because the $C_{16}K_3$ concentration in the electrogels is always around 5 wt.%, see below). We finally should mention that while the drying process may affect the morphology of the samples, the results in Figure 3 are fully consistent with the self-assembled C_nK_m nanofibers observed by SAXS and cryo-TEM in basic aqueous solutions in a previous study,[32] which supports the conclusion that our hydrogels are composed of elongated nanostructures of self-assembled PAs.

3.3. Effects of Deposition Variables

To characterize the electrodeposition methodology, we electrodeposited gels on gold disk electrodes (see Figure 2) by varying the applied potential or current, the deposition time, the initial pH, the ionic strength of the solution, and the chemical structure of the PA. To assess the influence of these parameters, we determined the height of the coating (as marked in Figure 2), the mass of the freshly prepared gel (m_{wg}), the dry mass (m_{dg}), and the weight % of water.

Figure 4A,C (top and center panels) show the height, dry mass (m_{dg}), and the mass of the freshly prepared gel (m_{wg}) coating as a function of the applied potential for gels deposited for 15 min from a 100 mM KNO_3, 2.5 wt.% $C_{16}K_3$ solution

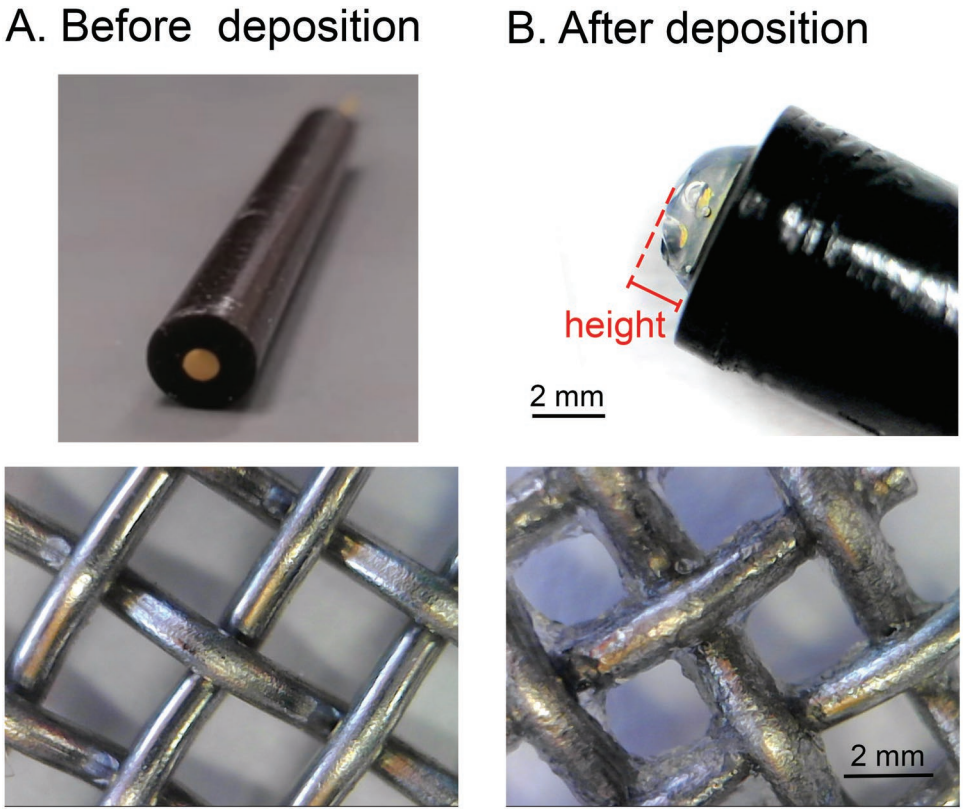

Figure 2. Images of a gold electrode (diameter = 3 mm) and a stainless-steel mesh (thread diameter = 1.3 mm) before and after the electrodeposition of a $C_{16}K_3$ gel. The height of the gel is marked with a red segment. Black bars indicate 2 mm.

and pH 9.2. The gel started to grow at a critical applied potential of approximately –1.1 V (against Ag/AgCl KCl 3 M), and then its height, dry mass, and mass of the freshly prepared gel increased with the modulus of the applied potential. The bottom panel of Figure 4C shows that the water weight percentage was around 95% and slightly increased with the modulus of the applied potential. Figure 4B shows the height of the gel as a function of the deposition time for an applied potential of –1.25 V. The gel height increased with time up to a point where it reached a plateau. This result is in line with previous experiments involving electrochemical depositions driven by a pH gradient.[23,71]

We also carried out galvanostatic depositions using different applied currents and deposition times. The obtained results were in line with those shown in Figure 4, that is, the height of the gel increased with the modulus of the applied current and the deposition time, reaching a plateau after 15 min in the latter case (see Figure S6, Supporting Information). For the following studies, we used potentiostatic deposition because galvanostatic deposition requires an accurate estimation of the electrode area to calculate the current density. Since potentiostatic deposition does not require this information, it is more convenient than galvanostatic deposition to deposit gels on electrodes of different shapes and dimensions.

The lower panel in **Figure 5**A shows that the dry mass of the gel decreases with decreasing solution pH. Interestingly, the water content of the gels was around 95 wt.% for all solution pHs. The amount of electrodeposited gel is also influenced by salt concentration. The upper panel of Figure 5B shows the mass of the deposited gel after drying (m_{dg}) as a function of NaCl concentration. On the other hand, the mass of the freshly prepared gel first increases and then decreases with salt concentration, see bottom panel of Figure 5B. This non-monotonic effect is relevant, but also rather complex, and it requires further mechanistic studies.

3.4. Mechanism of Electrodeposition

After studying the effects of the different processing variables, we addressed the mechanism of electrodeposition. We hypothesized the deposition is driven by the pH gradient that arises from the competition of the production of hydroxyl ions at the surface (originated in the water-reduction reaction, Equation (1)), and their diffusion into the bulk solution and acid-base neutralization by H^+ in the bulk. A similar diffusion-reaction mechanism was previously proposed for the pH-driven electrodeposition of chitosan.[71,72] Because the local pH decreases from the electrode surface to the bulk solution, we proposed that the height of the gel would reach a plateau with the deposition time (Figure 4B). This is because the gel will grow until it reaches a distance from the electrode at which the local pH is low enough to prevent gelation. This mechanism explains why changes in the experimental conditions that increase the rate of OH^- production, such as increasing the magnitude of the applied potential (Figure 4A,C) or current (Figure S6,

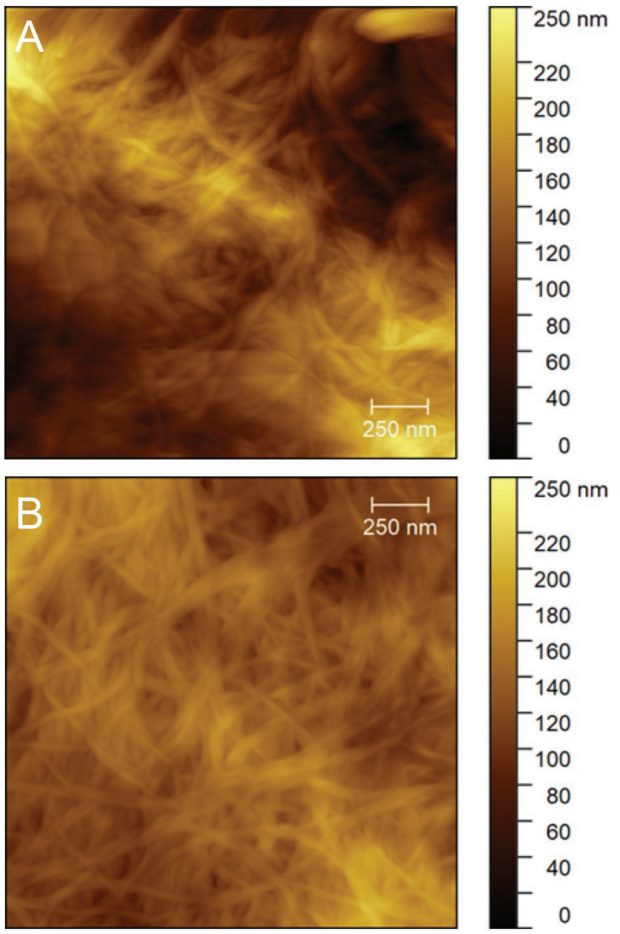

Figure 3. AFM height images of A) a chemical gel prepared by adding NaOH 1 M to a 5 wt.% $C_{16}K_3$ solution, and B) an electrodeposited $C_{16}K_3$ gel. The PA concentration in both gels was the same (≈5 wt.%).

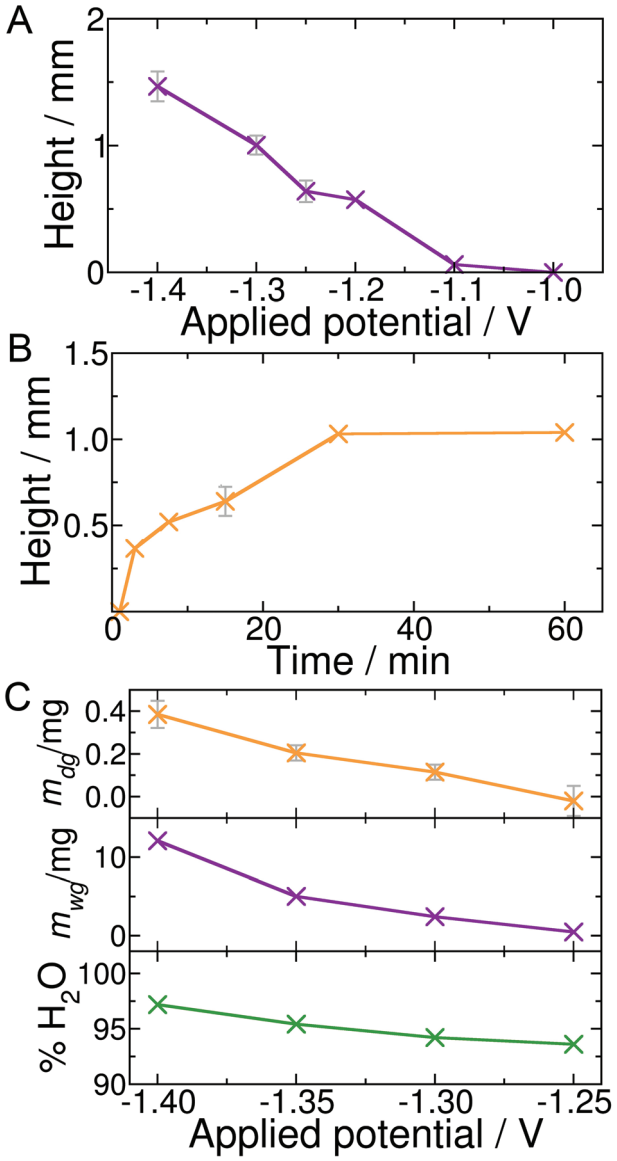

Figure 4. Height of an electrodeposited $C_{16}K_3$ gel on a planar gold electrode as a function of A) the applied potential (against Ag/AgCl KCl 3 M) and B) the deposition time. C) Dry mass (m_{dg}, top), the mass of the freshly prepared gel (m_{wg}, center), and water weight percentage (% H_2O, bottom) of an electrodeposited $C_{16}K_3$ gel as a function of the applied potential. In all cases, the gel was deposited from a 2.5 wt.% $C_{16}K_3$, 100 mM KNO_3, and pH 9.2 solution. Gels in (A) and (C) were deposited for 15 min. The applied potential in (B) was set to –1.25 V. The experiments were performed in duplicate (except in the cases where the error bars are not informed). Error bars indicate one standard deviation. Solid lines are guides to the eye.

Supporting Information), result in an increase in the amount of deposited gel. On the other hand, changes that promote the diffusion of OH^- away from the surface undermine the gel production; for example, we found that the agitation of the solution (200 rpm) fully prevented the gel deposition. This result is explained by the enhanced convective flow of OH^- from the electrode to the solution. Moreover, decreasing the bulk solution pH (Figure 5A) increases the rate of OH^- neutralization by bulk H^+ and, therefore, also hinders the electrodeposition process.

Despite the fact that we had previously demonstrated that the salt concentration does not have an effect on the sphere-to-fiber transition pH of $C_{16}K_3$ and $C_{16}K_2$,[31] this variable has an important and complex effect on electrodeposition (Figure 5B). We explain this apparently counterintuitive observation by analyzing the pH-driven gelation as a two-step process: the sphere-to-fiber transition, followed by the entanglement of the fibers to yield the gel. Only the second step is influenced by the ionic strength. As we discuss below, this mechanism also explains the fact that the sphere-to-fiber transition pHs for all compounds are lower than their respective gelation pHs (see **Table 1**).

3.5. Effect of the Chemical Structure of the PA on Electrodeposition and Properties of Hydrogel

Finally, we investigated the importance of the chemical structure of the PA. We first analyzed the behavior of $C_{16}K_3$, $C_{16}K_2$, and $C_{18}K_2$ solutions upon the addition of NaOH. The three compounds formed spherical micelles at low pH and transitioned to elongated structures with increasing pH (all formed

ADVANCED MATERIALS INTERFACES
Open Access
www.advmatinterfaces.de

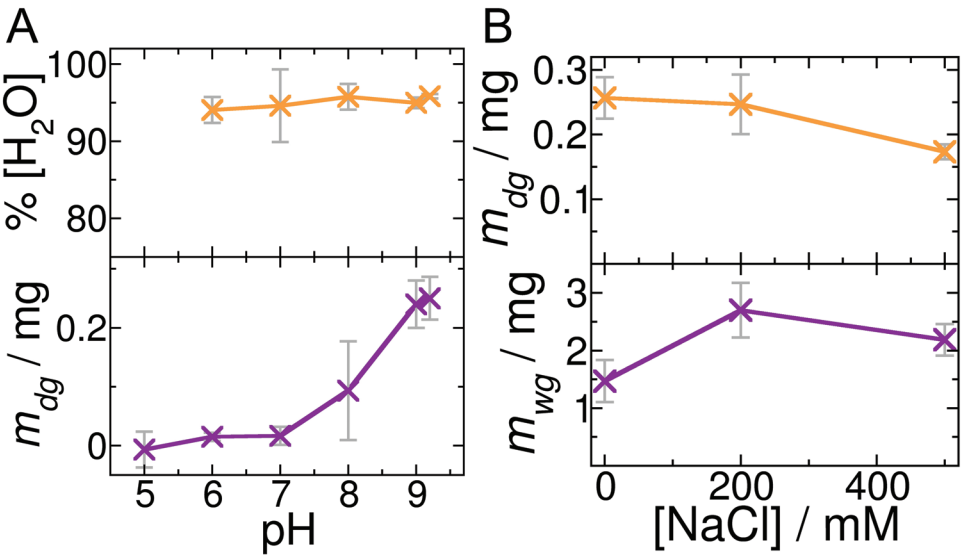

Figure 5. A) Water weight percentage (% H_2O, top) and dried gel mass (m_{dg}, bottom) of a $C_{16}K_3$ electrodeposited gel as a function of the pH of the solution. B) Dried gel mass (m_{dg}, top) and mass of the freshly prepared gel (m_{wg}, bottom) of an electrodeposited $C_{16}K_3$ gel as a function of the concentration of added NaCl. The gels were deposited by applying a potential of –1.3 V for 30 min. The pH was adjusted to 9.2 (panel (B). The experiments were performed in triplicate and the error bars indicate one standard deviation. Solid lines are guides to the eye.

cylindrical fibers first, while $C_{16}K_2$ and $C_{18}K_2$ also formed long, planar ribbons with further pH increase, see refs. [31,32], and Figure S5, Supporting Information). The transition pHs were 9, 7.5, and 6 for $C_{16}K_3$, $C_{16}K_2$, and $C_{18}K_2$, respectively. This result is in line with previous reports indicating that increasing the alkyl chain length ($C_{16}K_2$ vs $C_{18}K_2$) and/or decreasing the size and charge of the hydrophilic head ($C_{16}K_3$ vs $C_{16}K_2$) favor less curved structures like fibers and ribbons,[29,31,73] and thus cause a decrease in the transition pH. The gelation pH (pH_g) for 2.5 wt.% $C_{16}K_3$, $C_{16}K_2$, and $C_{18}K_2$ solutions were 10, 9.4, and 8.8, respectively. Note that the gelation pHs are higher than the sphere-to-fiber transition pHs, although both sets of pHs follow the same trend with the chemical structure of the PA (see Table 1). As we mentioned above, we believe that the gelation pH is higher than the transition pH because gelation follows a two-step process. The fibers formed at the sphere-to-fiber transition pH have a positive surface charge. This charge produces fiber-fiber repulsions that prevent entanglement. A further increase of the solution pH (i.e., a pH above the transition pH) deprotonates the lysines, decreases the surface charge, and, thus, allows entanglement. While a full theoretical treatment of this effect is outside the scope of this work, it is interesting to mention that the proposed mechanism is fully consistent with our previous theoretical studies of the role of surface charge on the aggregation of PA nanostructures (see Figure 5 in ref. [74]).

We studied the rheological properties of gels made of different PAs by oscillatory rheology, see Figure S4, Supporting Information. For all compounds, the storage modulus was higher than the loss modulus in the frequency range of 0.5–100 rad seg^{-1} and both were approximately constant with the frequency. The elastic modulus and the viscosity of the gels increased following the series $C_{16}K_3$ < $C_{16}K_2$ < $C_{18}K_2$ (see Table 1). This result can be explained by the fact that increasing the alkyl-chain length or decreasing the headgroup size and charge of the amphiphile increases the average length of the self-assembled fibers, thus lowering their relaxation times,[75] and, hence, increasing the cohesiveness of their gels.

In the previous paragraph, we showed how the properties of the PA gels depend on their chemical structure. We will now address how the structure affects the electrochemical deposition of the gels. Table 1 compares the masses of freshly made hydrogels electrodeposited from 2.5 wt.% $C_{16}K_3$, $C_{16}K_2$, and $C_{18}K_2$ solutions. In these experiments, we set the pHs of the solutions to the apparent pK_as of the lysines in each PA (9.2, 8.6, and 8.4, respectively, determined by acid-base titration), which are right below the pHs of gelation of each compound

Table 1. Summary of the physical properties of CnKm hydrogels.

PA	Sphere-to-fiber transition pH[a)]	Gelation pH[b)]	Apparent pKa[c)]	G′ [Pa][d)]	Electreposited mass [mg][e)]	% H_2O in electrodeposited films[e)]	Timescale of dissolution in PBS
$C_{16}K_3$	9	10	9.2	80	(5.2 ± 1.2)	95	≈hours
$C_{16}K_2$	7.5	9.4	8.6	1100	(2.7 ± 0.2)	92	N/D[f)]
$C_{18}K_2$	6	8.8	8.4	11 000	(2.3 ± 0.7)	90	≈weeks

[a)]Measured by TEM or cryo-TEM (see refs. [31,32] and Figure S5, Supporting Information); [b)]Measured by the inverted-vial test; [c)]Measured by acid-base titration; [d)]At 10 rad s^{-1}, see Figure S4, Supporting Information; [e)]Measured for gels freshly electrodeposited (wet) at pH = p*K*a, applied potential = –1.3 V, deposition time of 30 min and no added salt; [f)]N/D: Not determined.

(10, 9.4, and 8.8, respectively). In this way, the local pH increase needed to form the gel is approximately the same for all three compounds, so we can isolate the effect of the chemical structure from that of the solution pH. The masses of freshly prepared gels increased as follows: $C_{16}K_3 \lesssim C_{16}K_2 < C_{18}K_2$. We also measured the proportion of water in the gels, which were 95, 92, and 90 wt.% for $C_{16}K_3$, $C_{16}K_2$, and $C_{18}K_2$, respectively, and performed preliminary studies of the stability of electrodeposited gels in PBS solution. $C_{16}K_3$ gels dissolved completely after around 6 h of agitation at 37 °C, while $C_{18}K_2$ did not dissolve even after one week.

In summary, the results in Table 1 show that increasing the alkyl-chain length and decreasing the number of chargeable lysines result in an increase in the cohesive interactions of the systems. This increase in cohesiveness increases the electrodeposited mass (keeping all other variables fixed), decreases the hydration of the gel, and augments their stability (decreases their dissolution rate) in PBS. It also increases the stiffness and decreases the gelation pH for gels prepared by the direct addition of NaOH.

3.6. Antimicrobial Activity of PAs in Solution

We performed minimum inhibition concentration (MIC) assays of the three PAs in solution and at physiological pH and found that all were active against Gram-positive bacteria (methicillin-resistant *S. aureus*) and Gram-negative bacteria (*A. baumannii*, *E. coli*, and *P. aeruginosa*), see Table S1, Supporting Information. The MIC values were in the range of 4–16 μg mL^{-1} for *S. aureus*, *A. baumannii*, and *E. coli* and 16–32 μg mL^{-1} for *P. aeruginosa*. Our results for $C_{16}K_2$ and $C_{16}K_3$ were in line with those reported by Greber et al.[50] and Rodrigues et al.[42] It is worth mentioning that $C_{16}K_3$ is already used in personal care products as an antimicrobial agent under the name palmitoyl tripeptide-36.[46] To the best of our knowledge, $C_{18}K_2$ antimicrobial activity has not been studied in the past. This compound was slightly less active than the other two (particularly against Gram-negative bacteria). Greber et al. showed that increasing the length of the tail on the C_nK_m compounds led to an increase in the antimicrobial activity,[50] but for long alkyl chains, a non-monotonic effect of the length of the tail on the antimicrobial efficiency was observed.[42] We also studied the ability of the PA solutions to inhibit and destruct biofilms. We found that the solutions of the three compounds almost completely inhibited the growth of *S. aureus* biofilms at PA concentrations of 8–20 μg mL^{-1}, see Figure S7, Supporting Information. The PAs were also able to destroy around 50% of mature *S. aureus* biofilms at the same range of PA concentrations. Surprisingly, $C_{18}K_2$ solutions were more active against biofilms than $C_{16}K_3$ and $C_{16}K_2$. The mechanism of antimicrobial action and the toxicity of PAs of the family C_nK_m were already investigated by our group and others,[42,43,47,50,51] and thus they will not be addressed here.

3.7. Antimicrobial Activity of PA Hydrogels

To evaluate if the PA hydrogels retain the antimicrobial activity of the compounds in solution, we carried out adapted Kirby Bauer tests for chemical gels (formed by adding NaOH to a concentrated PA solution) and electrodeposited gels, following a procedure reported in the literature to study the antimicrobial activity of hydrogels.[64,65] The test consisted in placing ≈5 μL of the gel on the surface of a Muller–Hinton agar plate inoculated with bacteria. After overnight incubation, the diameter of the inhibition zone (if formed) was measured. The activity of the gels was compared against that of paper disks embedded only with a 1 M NaOH solution or deionized water. All PA gels showed activity against *S. aureus*, *E. coli*, and *P. aeruginosa* strains, while the disks with 1 M NaOH solution and deionized water were inactive. Hence, the antimicrobial activity of the gels can be exclusively attributed to the PAs. **Figure 6**A shows the inhibition zones against *S. aureus* of two $C_{16}K_2$ chemical gels (with PA concentrations of 2.5 and 10 wt.%, respectively) and one $C_{16}K_2$ electrogel (PA concentration of ≈5 wt.%). The three samples were active and produced inhibition zones. As

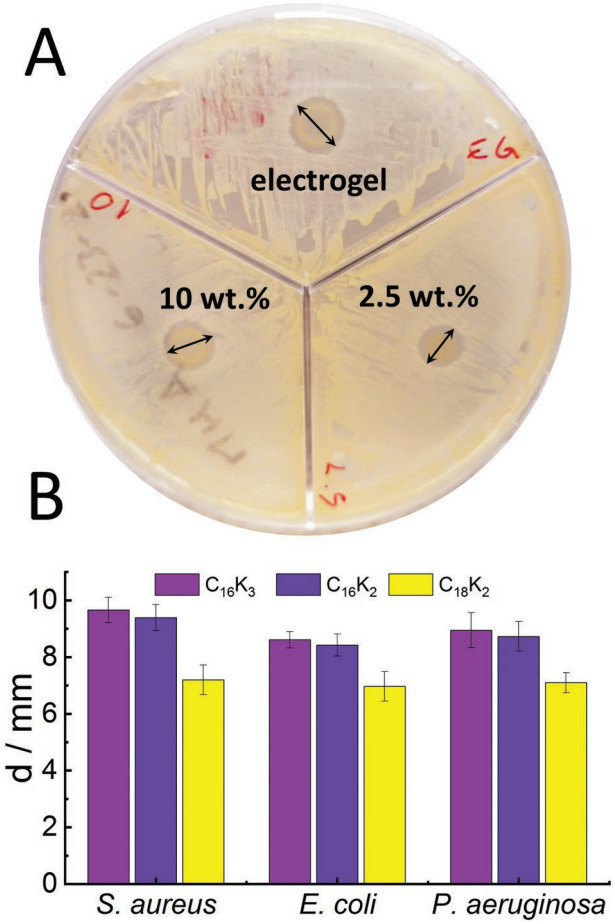

Figure 6. A) Inhibition zones of $C_{16}K_2$ gels against *S. aureus* for a gel electrodeposited from a 2.5 wt.% PA solution (approximate gel volume of 5 μL and PA concentration of 5 wt.%), and two chemical gels formed by adding NaOH to 5 μL of a PA solution with 2.5 and 10 wt.% PA concentration respectively. The diameters of the inhibition zone are marked with double arrows. B) Diameter of the inhibition zone (*d*) produced by $C_{16}K_3$, $C_{16}K_2$, and $C_{18}K_2$ 2.5 wt.% chemical gels against *S. aureus*, *E. coli*, and *P. aeruginosa*. The experiments were performed in triplicate and the error bars indicate one standard deviation.

expected, the activity of the chemical gels increased with the PA concentration.

To study how the chemical structure of the PA affects the antimicrobial activity of the gels, we performed Kirby Bauer tests of $C_{16}K_3$, $C_{16}K_2$, and $C_{18}K_2$ chemical gels against *S. aureus*, *E. coli*, and *P. aeruginosa*. Figure 6B shows the inhibition diameter, *d*, produced by gels with a concentration of 2.5 wt.% of the three compounds against the three strains. The gels were more active against *S. aureus* and *E. coli* than against *P. aeruginosa*, as expected from the MIC values (Table S4, Supporting Information). Interestingly, the antimicrobial activity generally increased in the order $C_{18}K_2 < C_{16}K_2 < C_{16}K_3$. This order does not correlate well with MIC values in solution (Table S1, Supporting Information), which were similar for the three compounds. We hypothesize that these differences in the activity are related to the rate of dissolution of the gels in aqueous media as discussed above, $C_{16}K_3$ dissolves much faster than $C_{18}K_2$ (see Table 1). This result could indicate that the activity shown by the Kirby Bauer test is controlled by the diffusion of the PA molecules from the gel to the media. PAs forming more stable gels diffuse at a lower rate and produce smaller inhibition zones.

3.8. Inhibition of Biofilm Formation by PA Hydrogels

To assess the impact of PA hydrogel coatings on bacterial biofilms, we measured the static biofilm formation by *P. aeruginosa* and *A. baumannii* (two pathogens prone to produce biofilms with antimicrobial resistance[76,77]) in a plate-based assay with gels coating the plate's surface. In this assay, we deposited hydrogels formed by $C_{18}K_2$, $C_{16}K_2$, and $C_{16}K_3$ into wells. We also prepared control samples by depositing aliquots of water and 1 M NaOH solutions into the wells. After washing, biofilms were grown for 24 h. The supernatants were then removed, the wells extensively washed and fresh media added. Bacterial growth after a further 18 h was measured both by OD_{600} value and, after centrifugal clarification, A_{490} (as an indicator of the production of bacterial chromophores). Our results (**Figure 7**) clearly demonstrate that the three compounds significantly reduced biofilm formation by *A. baumannii* and that the C_{16} compounds were also effective against *P. aeruginosa*, while $C_{18}K_2$ showed mixed results. The hydrogels of all three compounds persisted for the entire duration of the experiment. The mixed results obtained for $C_{18}K_2$ are surprising because the solution of this PA was more active (as a biofilm inhibitor) than the C_{16} compounds (Figure S7, Supporting Information). It is possible that the mixed performance of $C_{18}K_2$ hydrogels is related to their slow dissolution (high stability) compared to the other compounds. In this hypothesis (similar to that proposed above to explain the plate test results), $C_{18}K_2$ molecules diffuse more slowly from the hydrogel to the solution than the other compounds, and, thus they are less active against biofilm formation.

To confirm the effectivity of $C_{16}K_2$ and $C_{16}K_3$ to inhibit biofilm formation, we performed two additional surface-based assays. **Figure 8**A shows the quantification of *A. baumannii* biofilm formation by measuring their β-lactamase activity using nitrocefin.[66] We also studied the inhibition of *A. baumannii* colony formation on solid media selective for *A. baumannii* and related species (CHROMagar), which we impregnated with

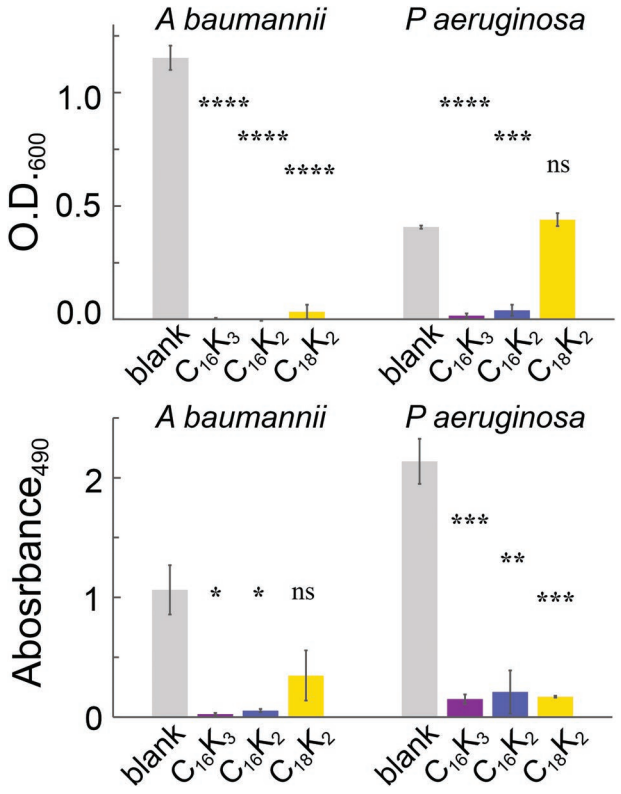

Figure 7. O.D.$_{600}$ (top) and A_{490} (bottom) measurements of the supernatant of bacterial cultures prepared in wells pretreated with the PA hydrogels where *A baumannii* and *P aeruginosa* biofilms were grown. Significant differences from the blank: * $p \leq 0.05$, ** $p \leq 0.01$, *** $p \leq 0.001$, **** $p \leq 0.0001$, ns: not significant (*p*-values calculated with Student's *t*-test, 2-tailed, unpaired).

$C_{16}K_2$ and $C_{16}K_3$ hydrogels (Figure 8B,C). These assays confirm that hydrogels of $C_{16}K_2$ and $C_{16}K_3$ inhibit the growth of *A. baumannii* on surfaces and solid media.

3.9. Cytotoxicity Studies of PA Solutions and Hydrogels

We evaluated the cytotoxicity profile of the three PAs both in solution and in the form of hydrogels against the epithelial type 2(HEp-2) cell line and the immortalized human embryonic kidney (HEK-293) cell line. In both cell lines, the three PAs in solution showed over 60% survival even at the highest concentration tested (128 µg/ml), see **Figure 9**A,B. The PAs $C_{16}K_2$ and $C_{16}K_3$ exhibited higher viabilities than $C_{18}K_2$. In the form of hydrogels, $C_{16}K_2$ and $C_{16}K_3$ led to a > 70% survival for both cell lines (Figure 9C), indicating an acceptable level of cell survival.[53] The fact that $C_{16}K_2$ displays a better cytotoxicity profile than $C_{18}K_2$ is consistent with our previous finding that shortening the hydrophobic tail can enhance cell viability.[42]

4. Conclusion

This study reports the first electrodeposited gels made of PAs and their application as antimicrobial coatings. PAs play a dual

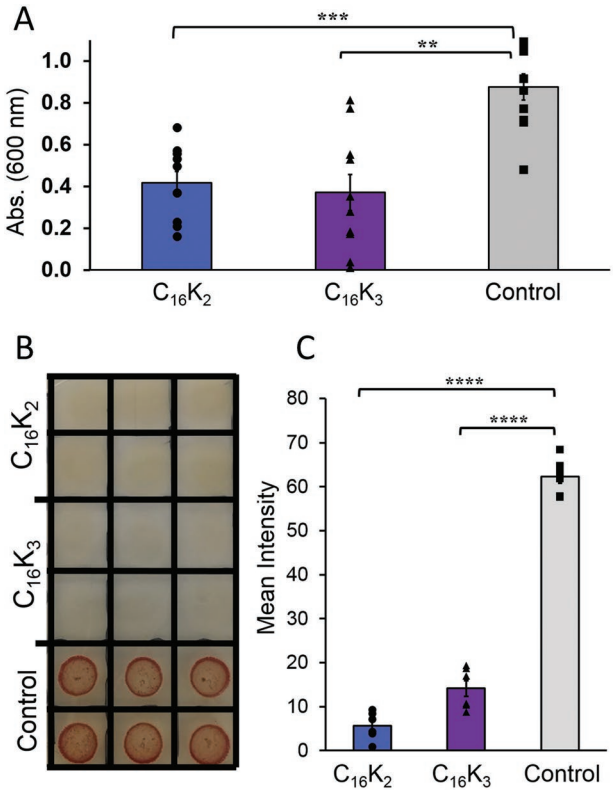

Figure 8. A) Inhibition of *A. baumannii* biofilm β-lactamase activity. β-lactamase activity from *A. baumannii* static biofilms grown in 96-well plates was measured using nitrocefin. Error bars mark the standard error. B) Inhibition of *A. baumannii* colony formation on CHROMagar Acinetobacter media. C) Quantification of *A. baumannii* colony formation by color intensity. Error bars mark the standard error. * $p \leq 0.05$, ** $p \leq 0.01$, *** $p \leq 0.005$, **** $p \leq 0.0005$.

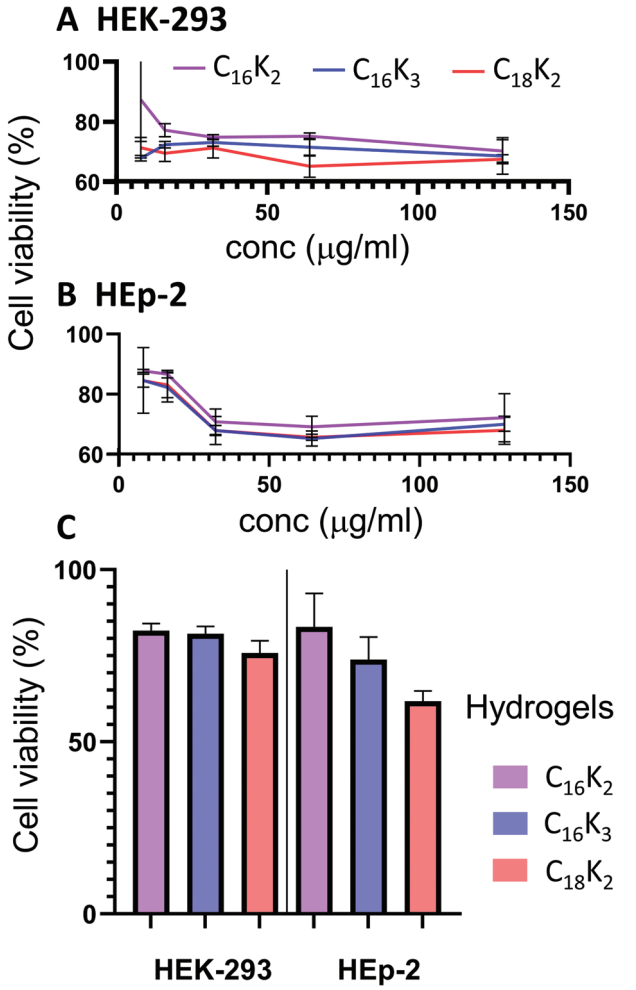

Figure 9. Cytotoxicity viability profile of A) PA solutions against HEK-293 cell line, B) PA solutions against HEp-2 cell line, and C) PA chemical gels against HEK-293 and HEp-2 cell lines. Error bars represent the standard error of the mean ($n = 3$). The error bar is clipped at the axis limit in (A).

role as both building blocks and antibiotic molecules, which is convenient as it simplifies the formulation of the hydrogel and allows to maximize the concentration of the bioactive compound. Electrodeposition allowed to produce films with tunable thickness that conformally adapt to complex-shaped surfaces.

Our electrodeposition method is based on the electrochemical generation of OH^- ions on the conductive surface, which triggers the sphere-to-fiber transition of the PAs. The entanglement of the produced fibers finally results in the deposition of the hydrogel on the surface. We performed a thorough study of the effect of the processing variables on the amount and composition of the electrodeposited gels. These studies revealed that electrodeposition is governed by a reaction-diffusion mechanism, in which increasing the rate of electrochemical production of OH^- ions (e.g., by increasing the electrode current) favors the deposition of the gel while accelerating the diffusion of OH^- (e.g., by mechanical agitation) or its acid-base neutralization by bulk H^+ (e.g., by lowering the bulk pH) hinders the formation of the gel. Our study also shows that the formation of the coating is a two-stage process involving the sphere-to-fiber transition followed by the entanglement of the formed fibers to produce the gel. The second process occurs at a pH that is 0.4–0.8 units higher than the first one, and it is benefited by the presence of added salt.

The electrochemical gels inhibited the growth of *S. aureus*, *E. coli*, and *P. aeruginosa* and prevented the formation of biofilms of *A. baumannii* and *P. aeruginosa*. The hydrogels of $C_{16}K_3$ and $C_{16}K_2$ displayed stronger antimicrobial activity than those of $C_{18}K_2$ and displayed > 70% cell viability for HEp-2 and HEK 293 cell lines, thus those compounds are the most promising for further studies.

Interestingly, while the hydrogels of $C_{16}K_3$ and $C_{16}K_2$ displayed the highest antimicrobial activity, the three PAs exhibited similar MICs in solution against *A. baumannii*, *S. aureus*, and *P. aeruginosa*. This discrepancy is explained by the fact that $C_{16}K_3$ and $C_{16}K_2$ hydrogels dissolve faster than those of $C_{18}K_2$. Notably, the rates of dissolution were controllable in a convenient range of hours to days by the chemical structure of the PA. This property is particularly interesting to control the rate of delivery and activity of the antibiotic PAs.

We envisage that the electrodeposition of PAs developed in this work can lead to antibacterial coatings for metal surgical implants and other medical materials. Furthermore, the headgroup of PAs can contain oligopeptides with different types of

biological functionalities (e.g., for regenerative medicine and drug delivery); thus our electrodeposition method combined with this design flexibility can open new routes to smart functional bio- and/or chemoactive coatings.

Supporting Information

Supporting Information is available from the Wiley Online Library or from the author.

Acknowledgements

G.Z. and J.F. contributed equally to this work. The authors thank Dr. Erin M. Gross for providing us access to potentiostats. M.T. and L.L. are fellows of CONICET. G.Z. acknowledge the Fulbright Commission and the University of Buenos Aires for travel grants. M.T. acknowledges financial support from Agencia Nacional de Promoción Científica y Tecnológica (ANPCyT) PICT-1520-2019. K.M.P.O. recognizes the Fulbright Visiting Professor Award. M.C.S. acknowledges support from the US Department of Defense-Peer Reviewed Medical Research Program 2017 (W81XWH-18-1-0113) and the National Science Foundation (CAREER, Award # 1941731). The authors acknowledge a CONICET-NIH Level 1 Bilateral Cooperation Grant.

Conflict of Interest

The authors declare no conflict of interest.

Data Availability Statement

The data that support the findings of this study are available in the supplementary material of this article.

Keywords

coatings, electrochemistry, fibers, micelles, reaction-diffusion, supramolecular chemistry

Received: January 17, 2023
Revised: March 15, 2023
Published online:

[1] A. T. B. Abadi, A. A. Rizvanov, T. Haertlé, N. L. Blatt, *J. Bionanosci.* **2019**, *9*, 778.
[2] T. G. Emori, R. P. Gaynes, *Clin. Microbiol. Rev.* **1993**, *6*, 428.
[3] C. Elliot, A. Justiz-Vaillant, *Int. Biol. Biomed. J.* **2018**, *4.2*, 72.
[4] Antibiotic resistance, https://www.who.int/news-room/fact-sheets/detail/antibiotic-resistance (accessed: July 2022).
[5] T. H. Jakobsen, S. R. Eickhardt, A. G. Gheorghe, C. Stenqvist, M. Sønderholm, C. Stavnsberg, P. Ø. Jensen, A. Odgaard, M. Whiteley, C. Moser, J. Hvolris, H. P. Hougen, T. Bjarnsholt, *APMIS* **2018**, *126*, 685.
[6] C. L. Ekegren, R. E. Climie, P. M. Simpson, N. Owen, D. W. Dunstan, W. Veitch, B. J. Gabbe, *Phys. Ther.* **2020**, *100*, 332.
[7] T. Lamagni, *J. Antimicrob. Chemother.* **2014**, *69*, i5.
[8] A. Salomé Veiga, J. P. Schneider, *Pept. Sci.* **2013**, *100*, 637.
[9] T. Bjarnsholt, *APMIS* **2013**, *121*, 1.
[10] R. Lace, K. G. Doherty, D. Dutta, M. D. P. Willcox, R. L. Williams, *Adv. Mater. Interfaces* **2020**, *7*, 2001232.
[11] T. Zhu, J. Mao, Y. Cheng, H. Liu, L. Lv, M. Ge, S. Li, J. Huang, Z. Chen, H. Li, L. Yang, Y. Lai, *Adv. Mater. Interfaces* **2019**, *6*, 1900761.
[12] G. Gaetano, P. Giuseppe, P. F. Salvatore, M. Susanna, S. Sara, R. C. Luca, in *Hydrogels*, Vol. *1* (Eds. S. Haider, A. Haider), IntehOpen, London, UK **2018**, Ch. 9.
[13] L.-Q. Wu, A. P. Gadre, H. Yi, M. J. Kastantin, G. W. Rubloff, W. E. Bentley, G. F. Payne, R. Ghodssi, *Langmuir* **2002**, *18*, 8620.
[14] E. R. Cross, *SN Appl Sci* **2020**, *2*, 397.
[15] C.-M. Xie, X. Lu, K.-F. Wang, F.-Z. Meng, O. Jiang, H.-P. Zhang, W. Zhi, L.-M. Fang, *ACS Appl. Mater. Interfaces* **2014**, *6*, 8580.
[16] C. Maerten, L. Jierry, P. Schaaf, F. Boulmedais, *ACS Appl. Mater. Interfaces* **2017**, *9*, 28117.
[17] D. Keskin, L. Tromp, O. Mergel, G. Zu, E. Warszawik, H. C. van der Mei, P. van Rijn, *ACS Appl. Mater. Interfaces* **2020**, *12*, 57721.
[18] X. Pang, I. Zhitomirsky, *Surf. Coat. Technol.* **2008**, *202*, 3815.
[19] F. Pishbin, V. Mouriño, J. B. Gilchrist, D. W. McComb, S. Kreppel, V. Salih, M. P. Ryan, A. R. Boccaccini, *Acta Biomater.* **2013**, *9*, 7469.
[20] Y. Wang, X. Guo, R. Pan, D. Han, T. Chen, Z. Geng, Y. Xiong, Y. Chen, *Mater. Sci. Eng., C* **2015**, *53*, 222.
[21] J. Raeburn, B. Alston, J. Kroeger, T. O. McDonald, J. R. Howse, P. J. Cameron, D. J. Adams, *Mater. Horiz.* **2014**, *1*, 241.
[22] E. K. Johnson, D. J. Adams, P. J. Cameron, *J. Am. Chem. Soc.* **2010**, *132*, 5130.
[23] V. Lakshminarayanan, L. Poltorak, E. J. R. Sudhölter, E. Mendes, J. van Esch, *Electrochim. Acta* **2020**, *350*, 136352.
[24] H. Cui, M. J. Webber, S. I. Stupp, *Pept. Sci.* **2010**, *94*, 1.
[25] J. D. Hartgerink, E. Beniash, S. I. Stupp, *Science* **2001**, *5547*, 1684.
[26] M. P. Hendricks, K. Sato, L. C. Palmer, S. I. Stupp, *Acc. Chem. Res.* **2017**, *50*, 2440.
[27] M. Conda-Sheridan, S. S. Lee, A. T. Preslar, S. I. Stupp, *Chem. Commun.* **2014**, *50*, 13757.
[28] T. Gore, Y. Dori, Y. Talmon, M. Tirrell, H. Bianco-Peled, *Langmuir* **2001**, *17*, 5352.
[29] X.-D. Xu, Y. Jin, Y. Liu, X.-Z. Zhang, R.-X. Zhuo, *Colloids Surf., B* **2010**, *81*, 329.
[30] J. E. Goldberger, E. J. Berns, R. Bitton, C. J. Newcomb, S. I. Stupp, *Angew. Chem., Int. Ed.* **2011**, *50*, 6292.
[31] G. Zaldivar, S. Vemulapalli, V. Udumula, M. Conda-Sheridan, M. Tagliazucchi, *J. Phys. Chem. C* **2019**, *123*, 17606.
[32] C. Gao, H. Li, Y. Li, S. Kewalramani, L. C. Palmer, V. P. Dravid, S. I. Stupp, M. Olvera de la Cruz, M. J. Bedzyk, *J. Phys. Chem. B* **2017**, *121*, 1623.
[33] Z. Álvarez, A. N. Kolberg-Edelbrock, I. R. Sasselli, J. A. Ortega, R. Qiu, Z. Syrgiannis, P. A. Mirau, F. Chen, S. M. Chin, S. Weigand, E. Kiskinis, S. I. Stupp, *Science* **2021**, *374*, 848.
[34] R. N. Shah, N. A. Shah, M. M. D. R. Lim, C. Hsieh, G. Nuber, S. I. Stupp, *Proc. Natl. Acad. Sci. U. S. A.* **2010**, *107*, 3293.
[35] L. C. Palmer, C. J. Newcomb, S. R. Kaltz, E. D. Spoerke, S. I. Stupp, *Chem. Rev.* **2008**, *108*, 4754.
[36] R. Zhang, J. D. Smith, B. N. Allen, J. S. Kramer, M. Schauflinger, B. D. Ulery, *ACS Biomater. Sci. Eng.* **2018**, *4*, 2463.
[37] M. J. Webber, J. Tongers, M.-A. Renault, J. G. Roncalli, D. W. Losordo, S. I. Stupp, *Acta Biomater.* **2010**, *6*, 3.
[38] J. B. Matson, S. I. Stupp, *Chem. Commun.* **2011**, *47*, 7962.
[39] T. J. Moyer, H. A. Kassam, E. S. Bahnson, C. E. Morgan, F. Tantakitti, T. L. Chew, M. R. Kibbe, S. I. Stupp, *Small* **2015**, *11*, 2750.
[40] S. M. Standley, D. J. Toft, H. Cheng, S. Soukasene, J. Chen, S. M. Raja, V. Band, H. Band, V. L. Cryns, S. I. Stupp, *Cancer Res.* **2010**, *70*, 3020.
[41] D. J. Toft, T. J. Moyer, S. M. Standley, Y. Ruff, A. Ugolkov, S. I. Stupp, V. L. Cryns, *ACS Nano* **2012**, *6*, 7956.
[42] N. Rodrigues de Almeida, Y. Han, J. Perez, S. Kirkpatrick, Y. Wang, M. C. Sheridan, *ACS Appl. Mater. Interfaces* **2018**, *11*, 2790.

[43] A. Makovitzki, J. Baram, Y. Shai, *Biochemistry* **2008**, *47*, 10630.
[44] B. Mishra, T. Lushnikova, G. Wang, *RSC Adv.* **2015**, *5*, 59758.
[45] S. K. Schagen, *Cosmetics* **2017**, *4*, 16.
[46] Safety Assessment of Palmitoyl Oligopeptides Ingredients as Used in Cosmetics | Cosmetic Ingredient Review, https://www.cir-safety.org/panelbook/safety-assessment-palmitoyl-oligopeptides-ingredients-used-cosmetics (accessed: July 2022).
[47] G. Shahane, W. Ding, M. Palaiokostas, H. S. Azevedo, M. Orsi, *J. Membr. Biol.* **2019**, *252*, 317.
[48] W. C. Wimley, *ACS Chem. Biol.* **2010**, *5*, 905.
[49] Y. Niu, S. Padhee, H. Wu, G. Bai, Q. Qiao, Y. Hu, L. Harrington, W. N. Burda, L. N. Shaw, C. Cao, J. Cai, *J. Med. Chem.* **2012**, *55*, 4003.
[50] K. E. Greber, J. Zielińska, Ł. Nierzwicki, K. Ciura, P. Kawczak, J. Nowakowska, T. Bączek, W. Sawicki, *Biochim. Biophys. Acta* **2019**, *1861*, 93.
[51] K. E. Greber, M. Dawgul, W. Kamysz, W. Sawicki, *Front. Microbiol.* **2017**, *8*, 123.
[52] G. Tao, R. Cai, Y. Wang, H. Zuo, H. He, *Mater. Sci. Eng., C* **2021**, *119*, 111597.
[53] V. Gribova, F. Boulmedais, A. Dupret-Bories, C. Calligaro, B. Senger, N. E. Vrana, P. Lavalle, *ACS Appl. Mater. Interfaces* **2020**, *12*, 19258.
[54] K. B. Steinbuch, M. Fridman, *MedChemComm* **2016**, *7*, 86.
[55] R. E. Hancock, *Lancet* **1997**, *349*, 418.
[56] M. N. Alekshun, S. B. Levy, *Cell* **2007**, *128*, 1037.
[57] E. J. Chung, L. B. Mlinar, M. J. Sugimoto, K. Nord, B. B. Roman, M. Tirrell, *Nanomed.: Nanotechnol. Biol. Med.* **2015**, *11*, 479.
[58] M. B. Samad, Y. S. Chhonker, J. I. Contreras, A. McCarthy, M. M. McClanahan, D. J. Murry, M. Conda-Sheridan, *Macromol. Biosci.* **2017**, *17*, 1700096.
[59] C. H. Chen, L. C. Palmer, S. I. Stupp, *Nano Lett.* **2018**, *18*, 6832.
[60] B. Joddar, Y. Ito, *J. Mater. Chem.* **2011**, *21*, 13737.
[61] D. R. Bijukumar, C. McGeehan, M. T. Mathew, *Curr. Osteoporosis Rep.* **2018**, *16*, 236.
[62] J. N. Cabrera, M. M. Ruiz, M. Fascio, N. D'Accorso, R. Mincheva, P. Dubois, L. Lizarraga, R. M. Negri, *Polymers* **2017**, *9*, 331.
[63] C. A. Schneider, W. S. Rasband, K. W. Eliceiri, *Nat. Methods* **2012**, *9*, 671.
[64] L. Fan, J. Yang, H. Wu, Z. Hu, J. Yi, J. Tong, X. Zhu, *Int. J. Biol. Macromol.* **2015**, *79*, 830.
[65] S. Atefyekta, E. Blomstrand, A. K. Rajasekharan, S. Svensson, M. Trobos, J. Hong, T. J. Webster, P. Thomsen, M. Andersson, *ACS Biomater. Sci. Eng.* **2021**, *7*, 1693.
[66] C. H. O'Callaghan, A. Morris, S. M. Kirby, A. H. Shingler, *Antimicrob. Agents Chemother.* **1972**, *1*, 283.
[67] L. Kamentsky, T. R. Jones, A. Fraser, M.-A. Bray, D. J. Logan, K. L. Madden, V. Ljosa, C. Rueden, K. W. Eliceiri, A. E. Carpenter, *Bioinformatics* **2011**, *27*, 1179.
[68] G. H. A. Therese, P. V. Kamath, *Chem. Mater.* **2000**, *12*, 1195.
[69] C.-Y. Leung, L. C. Palmer, S. Kewalramani, B. Qiao, S. I. Stupp, M. O. De La Cruz, M. J. Bedzyk, *Proc. Natl. Acad. Sci. USA* **2013**, *110*, 16309.
[70] G. Changrui, *Electrostatically Driven Transformation in Assembly of Charged Amphiphiles*, Ph.D. Thesis, Northwestern University, Evanston, IL **2008**.
[71] Y. Cheng, X. Luo, J. Betz, S. Buckhout-White, O. Bekdash, G. F. Payne, W. E. Bentley, G. W. Rubloff, *Soft Matter* **2010**, *6*, 3177.
[72] K. Yan, Y. Liu, J. Zhang, S. O. Correa, W. Shang, C.-C. Tsai, W. E. Bentley, J. Shen, G. Scarcelli, C. B. Raub, X.-W. Shi, G. F. Payne, *Biomacromolecules* **2018**, *19*, 364.
[73] G. Zaldivar, M. B. Samad, M. Conda-Sheridan, M. Tagliazucchi, *Soft Matter* **2018**, *14*, 3171.
[74] H. Xing, S. M. Chin, V. R. Udumula, M. Krishnaiah, N. Rodrigues de Almeida, C. Huck-Iriart, A. S. Picco, S. R. Lee, G. Zaldivar, K. A. Jackson, M. Tagliazucchi, S. I. Stupp, M. Conda-Sheridan, *Biomacromolecules* **2021**, *22*, 3274.
[75] C. A. Dreiss, Y. Feng, *Wormlike Micelles: Advances in Systems, Characterisation and Applications*, Royal Society of Chemistry, London **2017**.
[76] E. Drenkard, *Microbes Infect* **2003**, *5*, 1213.
[77] D. L. Wannigama, C. Hurst, L. Pearson, T. Saethang, U. Singkham-in, S. Luk-in, R. J. Storer, T. Chatsuwan, *Sci. Rep.* **2019**, *9*, 6300.